Rock Mechanics and Rock Engineering (2023) 56:7129–7146
https://doi.org/10.1007/s00603-023-03248-9

ORIGINAL PAPER

Quantitative Evaluation of the Effects of Input Parameter Heterogeneity on Model Behavior for Bonded Block Models of Laboratory Rock Specimens

Isabella West[1] · **Gabriel Walton**[1]

Received: 18 March 2022 / Accepted: 24 January 2023 / Published online: 6 February 2023

Abstract

Bonded block models (BBMs) have become increasingly common for simulation of laboratory-scale rock samples in unconfined compressive strength and triaxial compression tests. BBMs require input parameters that describe the deformation of the blocks themselves (block properties), as well as the interactions between blocks (contact properties). Previous studies have found that incorporating heterogeneity of input parameters into BBMs is necessary to match all attributes of rock behavior, but little is known about the specific effects that the heterogeneity of these properties have on individual aspects of the overall behavior of the BBM. Therefore, this study presents a parametric study on the heterogeneity of elastic block and contact input parameters. Such input parameters were tested separately by varying the degree of heterogeneity between block or contact types, while keeping the weighted average of each given property constant for all simulations. Trends were analyzed for simulations under unconfined and confined conditions with 12 MPa of pressure. Rock specimen properties were computed from the model results including Young's modulus, Poisson's ratio, unconfined compressive strength and peak strength, crack initiation (CI) and crack damage (CD) parameters, and peak dilation angle. While several minor influences of heterogeneity on macroscopic properties were noted, the primary influence was that of contact peak cohesion heterogeneity on CD. Additionally, while the heterogeneity of no individual parameter was found to influence CI, when degrees of heterogeneity for all parameters were varied simultaneously, this had a significant effect on CI (as well as CD).

Highlights

- Compression test simulations were run on a laboratory-scale bonded block models (BBMs) of Blanco Mera Granite.
- Sensitivity analyses were performed to investigate the effects that the heterogeneity of each input parameter has on the emergent behavior of the model.
- Contact peak cohesion has a notable effect on the unconfined compressive strength and crack damage stress of the model.
- The crack initiation stress was relatively insensitive to changes in individual model parameters, but responded to a simultaneous increase in heterogeneity of multiple parameters.

Keywords Bonded block models · UDEC voronoi · Rock fracturing · Micromechanical input parameters · Heterogeneity

1 Introduction

Numerical models are commonly used to study rock behavior. Numerical models can be used to complement laboratory testing, as they require less labor to complete. Unconfined compressive strength (UCS) and triaxial tests are laboratory tests that are commonly used to assess the material properties of intact rock. Bonded block models (BBMs) can be used to simulate such laboratory tests where the models are

✉ Isabella West
igwest@mines.edu

Gabriel Walton
gwalton@mines.edu

[1] Department of Geology and Geological Engineering, Colorado School of Mines, Golden, CO, USA

created to match the composition of a rock at the grain scale (Farahmand and Diederichs 2015; Li et al. 2017; Sinha and Walton 2020). BBMs can then be further applied to field-scale modeling scenarios such as roof stability, pillar design, and other scenarios that cannot be easily tested in a laboratory (Garza-Cruz et al. 2014, 2019; Sinha and Walton 2021).

BBMs correspond to a subset of discrete element method (DEM) modeling where material is broken into a set of distinct, continuous elements that are bonded to and interact with each other. In the case of BBMs, these elements represent individual mineral grains. The deformations of the continuous elements, as well as their interaction with adjacent elements, are governed by a series of input parameters (Jing 2003). Each input parameter affects the model's macroscopic behavior uniquely, and many studies have previously analyzed the effect that the variation of these input parameters has on the macroscopic behavior of the model (Bahaaddini and Rahimi 2018; Cai and Noorani 2015; Ghazvinian et al. 2014; Wang and Cai 2019). Note, however, that while the sensitivity analyses presented in these previous studies considered the influences of overall parameter values, they did not specifically isolate the effects of parameter heterogeneity.

BBMs use polygonal blocks as the continuous elements, which can be modeled as rigid, elastic, or inelastic (Ghazvinian et al. 2014). Elastic blocks have been the most commonly used in the literature, but models with inelastic blocks have been found to more accurately replicate the behavior of intact rock, particularly in the post-peak regime and under higher confinements (Sinha and Walton 2020). BBMs are commonly used for modeling intact rock because the polygonal blocks can be generated with specified sizes and shapes that can reasonably approximate the grain structure of low-porosity rocks (Contreras Inga et al. 2021). Furthermore, the interaction of the blocks with adjacent ones is analogous to the interaction between mineral grains within real rock. Contacts within DEMs can break, simulating the loss of strength that occurs at grain-to-grain contacts in rock as damage accumulates.

Polymineralic rocks are composed of more than one mineral type, each of which can be represented in a BBM as a different block type with its own set of input parameters (Lan et al. 2010; Li et al. 2019; Nicksiar and Martin 2014). For elastic block BBMs, these parameters are density, Young's modulus, and Poisson's ratio. Density is a well-constrained property, as it is easily determined in the laboratory. Although the elastic moduli input parameters can also be deduced via laboratory experiments (Bass 1995), there is often some variability in these properties due to weathering, preexisting flaws in the crystal lattice, etc. (Saito 1981; Shen et al. 2019). Additionally, for polymineralic BBMs, there exists more than one type of contact between blocks, each of which requires a different set of input parameters (Chen et al. 2016). Previous studies have found that incorporating this heterogeneity of block contact properties is necessary to match all attributes of rock behavior (Sinha and Walton 2020), but little is known about the effect of heterogeneity of specific contact properties on individual aspects of the overall mechanical behavior of the BBM. Unlike density and elastic moduli, contact properties cannot be measured in the laboratory and must be back-calculated via a calibration process. This calibration process entails varying contact and block input parameters until the macroscopic behavior of the BBM matches laboratory data (Wang and Cai 2019). The more contact types that exist in a BBM, the more unique inputs the model requires for calibration. Different values for the same input parameter can be used for each contact type. This variation in values of each input parameter affects the model's behavior (Chen and Konietzky 2014).

With all this in mind, this paper documents a parametric study on the heterogeneity of elastic block moduli and contact input parameters, as applied to the individual elements of the bonded block model. Specifically, by keeping the weighted averages of all model properties constant between simulations, the specific effects of heterogeneity were isolated. A BBM with elastic blocks was considered rather than one with inelastic blocks due to model run-time considerations and because elastic BBMs are more widely used (Sinha and Walton 2020). The contact parameters considered in the study were normal and shear stiffnesses, peak cohesion, peak friction angle, peak tensile strength, residual friction angle, and dilation angle. Although BBMs require residual cohesion and residual tensile strength inputs as well, these were not considered, as they are commonly set to zero for brittle rock (Ghazvinian et al. 2014; Park et al. 2017; Stavrou and Murphy 2018; Wang and Cai 2019). Trends in macroscopic material properties as a function of elastic block and contact parameter heterogeneity were analyzed for each model, which are: Young's modulus, Poisson's ratio, crack initiation (CI) and crack damage (CD) parameters, UCS and peak strength, and peak dilation angle.

2 Model Setup

A previously developed elastic block BBM of Blanco Mera granite (West et al. 2020) generated in Neper Polycrystal (Quey et al. 2011) and Itasca's UDEC softwares and then calibrated to laboratory data (Alejano et al. 2017; Walton et al. 2018) was used as a basis for this study. Blanco Mera granite contains four different major mineral types (plagioclase, quartz, alkali feldspar, and mica) and therefore contains ten distinct contact types, as shown in Fig. 1.

Data on the shape and grain size distributions of each mineral, as well as the proportions of the minerals in the rock were provided by an unpublished petrology report (University of Vigo 2011). The blocks of the BBM were assigned

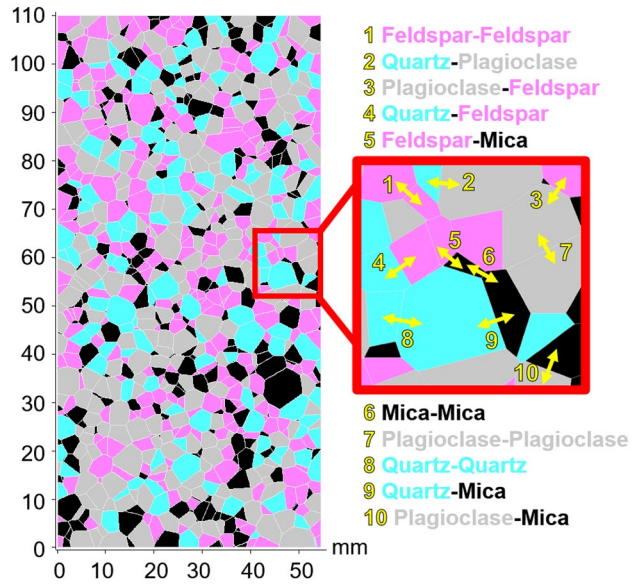

Fig. 1 The BBM of Blanco Mera granite used in this study. It contains four mineral (block) types: feldspar, quartz, plagioclase, and mica. 10 unique contact types exist, labeled in yellow (Color figure online)

to a mineral type so that the sizes, shapes, and proportions of minerals in the model matched those reported for Blanco Mera granite (see Table 1).

A complete description of the BBM block generation and mineral grain assignment for the Blanco Mera BBM is provided by West et al. (2020). Additionally, discussion on the assignment of block density is included there.

All BBMs must be calibrated to laboratory data via an iterative process of varying input parameters until the emergent behavior approximates that of the laboratory rock specimens. A preliminary calibration of the Blanco Mera BBM was presented by West et al. (2020); some adjustments to the calibration have been made since that time. The calibration process used in this study involved modifying model input parameters by a trial-and-error process to match emergent specimen-scale model properties to values obtained from laboratory testing. The following material attributes were considered as calibration targets under unconfined conditions and confining stress up to 12 MPa: Young's modulus, Poisson's ratio, crack initiation and crack damage thresholds, and peak strength. Details of the calibration process as well as the final calibrated model results were previously published by West et al. (2020). Note that post-peak rock stress–strain behavior cannot be reproduced by the type of BBM considered (i.e., with an elastic constitutive model applied to the blocks (Sinha and Walton 2020)), so only pre-peak material attributes and peak strength were used for calibration. Figure 2 includes the calibration results of the BBM used for this study plotted with the laboratory data to which it was calibrated. The calibrated model input parameters are presented in Tables 2 and 3, as they were used as the basis for this study.

Normal and shear stiffness inputs dictate the amount of normal and shear displacement that occur at a contact under a given stress level. Peak cohesion and peak friction angle dictate the compressional strength of the contact as per the Mohr–Coulomb constitutive model (Fabjan et al. 2015), where a contact will fail (i.e., forms a shear crack between blocks) once the strength of the contact is exceeded. Peak tensile strength defines the tensile stress state at which a contact will fail (i.e., forms a tensile crack between blocks). Once a contact fails, its behavior becomes governed by residual strength parameters (residual cohesion, residual friction angle, and residual tensile strength) which are defined in the same way as their peak parameter counterparts. Dilation angle dictates the amount of normal displacement that is induced as shear displacement occurs across a closed contact, which in turn increases the normal force on the contact (Itasca 2014).

These base input parameter values (listed in Tables 2 and 3) were varied such that the individual values were specifically chosen to correspond to a quantifiable increase or decrease in heterogeneity across either block or contact types.

The goal of this parametric study was to isolate the influence of input parameter heterogeneity, while keeping the mean value of each property constant for all simulations. Therefore, a heterogeneity factor was defined to quantify the degree of parameter heterogeneity relative to the base parameter set and the weighted average input value. A new value ($Value_f$) for each block or contact's input parameter can, thus, be calculated based on the original parameter from

Table 1 The BBM's average grain diameters and proportions for each mineral group compared to those of the real rock (West et al. 2020)

Mineral group	Rock proportion (%)	BBM proportion (%)	Rock average grain diameter (mm)	BBM average block diameter (mm)
Plagioclase	37	37.03	3.5	3.50
Quartz	20	20.18	3.5	3.47
Alkali Feldspar	27	27.12	3.0	2.65
Mica	16	15.66	1.9	1.91

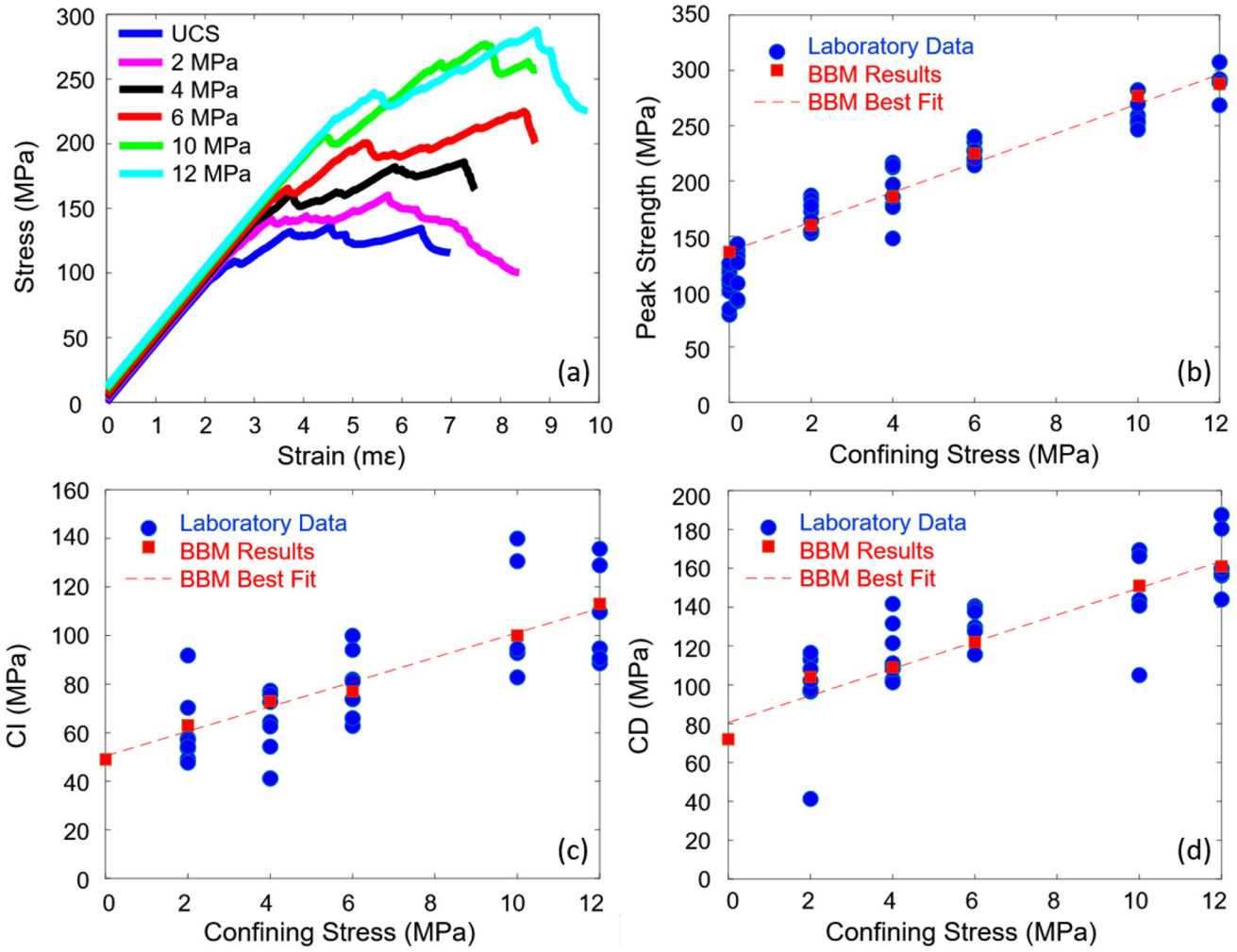

Fig. 2 Results of the calibrated BBM from West et al. (2020). **a** Stress–strain curves of the model under the range of confinement levels to which the model was calibrated. Note that the strain hardening between CD and the peak strength as well as the post-peak behavior have not been calibrated. **b** Peak strength. **c** Crack initiation (CI). **d** Crack damage (CD)

Table 2 Mineral group densities and elastic moduli values assigned to blocks within the Blanco Mera BBM

Mineral group	Property	Value	Unit
Plagioclase	Density	2630	kg/m^3
	Young's modulus (E)	72.11	GPa
	Poisson's ratio (ν)	0.28	–
Quartz	Density	2650	kg/m^3
	Young's modulus (E)	95.57	GPa
	Poisson's ratio (ν)	0.08	–
Alkali feldspar	Density	2650	kg/m^3
	Young's modulus (E)	73.49	GPa
	Poisson's ratio (ν)	0.28	–
Mica	Density	3050	kg/m^3
	Young's modulus (E)	88.09	GPa
	Poisson's ratio (ν)	0.25	–

the base case (listed in Tables 2 and 3), a specified heterogeneity factor (HF), and the weighted average (WA) of the contact values (see Eq. 1).

$$\text{Value}_f = \text{WA} + \text{HF} * (\text{Value}_0 - \text{WA}) \quad (1)$$

where Value_f is the new value for a given input parameter, Value_0 is the original value used in the base BBM (per Tables 2 or 3), and WA is the weighted average of the blocks' or contacts' values for a given input parameter. A heterogeneity factor greater than 1 indicates an increase in heterogeneity from the base model and a factor less than 1 indicates a decrease in heterogeneity from the base model.

The weighted average is calculated by multiplying each of the base block (Table 2) or contact (Table 3) property values by their respective proportions, and then summing these numbers. Table 4 shows the proportions of the four block

Table 3 Micro-parameters of the base BBM from West et al. (2020) with a modified calibration to laboratory data (Alejano et al. 2017; Walton et al. 2018)

Property/contact	jkn (GPa/m)	jks (GPa/m)	c (MPa)	Φ (°)	jt (MPa)	c_{res} (MPa)	Φres (°)	jt_{res} (MPa)	Ψ (°)
Mica–Mica	3.3E+04	1.3E+04	46.6	56.5	29.5	0	3.0	0	5.0
Quartz–Quartz	7.1E+04	2.8E+04	75.8	63.5	40.8	0	3.0	0	5.0
Plagioclase–Plagioclase	6.3E+04	2.5E+04	65.3	61.5	43.2	0	3.0	0	5.0
Feldspar–Feldspar	5.8E+04	2.3E+04	64.2	61.5	40.8	0	3.0	0	5.0
Quartz–Plagioclase	5.8E+04	2.3E+04	52.4	58.5	24.6	0	3.0	0	5.0
Quartz–Mica	5.8E+04	2.3E+04	46.6	53.5	93.4	0	3.0	0	5.0
Plagioclase–Mica	5.8E+04	2.3E+04	31.5	53.5	26.2	0	3.0	0	5.0
Plagioclase–Feldspar	5.3E+04	2.1E+04	63.0	58.5	37.4	0	3.0	0	5.0
Feldspar–Mica	5.8E+04	2.3E+04	35.0	53.5	13.3	0	3.0	0	5.0
Feldspar–Quartz	6.8E+04	2.7E+04	44.3	58.5	33.0	0	3.0	0	5.0

Definitions of parameter abbreviations are: jkn = normal stiffness, jks = shear stiffness, c = cohesion, ϕ = friction angle, jt = tensile strength, c_{res} = residual cohesion, jt_{res} = residual tensile strength, Ψ = dilation angle

Table 4 Percentages of block types within the Blanco Mera granite BBM (West et al. 2020)

Mineral group	Proportion in BBM (%)
Plagioclase	37
Quartz	20
Alkali Feldspar	27
Mica	16
Total	100

Table 5 Percentages of contact types within the Blanco Mera granite BBM (West et al. 2020)

Contact type	Percentage (%)
Mica–Mica	4.8
Quartz–Quartz	2.3
Plagioclase–Plagioclase	9.1
Feldspar–Feldspar	8.6
Quartz–Plagioclase	12.4
Mica–Quartz	7.6
Mica–Plagioclase	12.5
Feldspar–Plagioclase	20.0
Mica–Feldspar	13.0
Feldspar–Quartz	9.7
Total	100.00

types and Table 5 shows the proportions of the ten contact types within the Blanco Mera granite BBM.

A visual example of this Heterogeneity Factor (HF) is shown in Fig. 3, where four HFs are included to show how the spread of input parameter values vary as a function of HF. In this example, larger HFs result in a larger spread of peak tensile strength values. HF = 0 results in all contacts assigned the same value, which is equal to the weighted

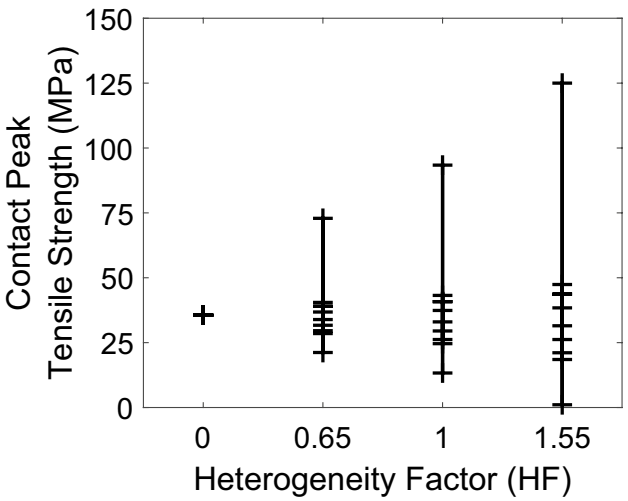

Fig. 3 Example of how the heterogeneity factor (HF) influences the spread of input parameter values. This example is for contact peak tensile strength, with values for each contact type marked with ticks

average (WA in Eq. 1). HF = 1 is the base case (see Tables 2 and 3).

Simulations of UCS and triaxial tests were run on the Blanco Mera BBM by varying the HF for each input parameter, one at a time. These varied values were calculated using Eq. 1 with specified heterogeneity factors. All other input parameters were kept equal to their values from the calibrated base model as per Tables 2 and 3.

At least ten heterogeneity factors (HFs) were tested for each input parameter. More than ten HFs were tested for the block moduli inputs to investigate unique trends identified from initial models. The ranges of the HFs chosen were dictated by the constraint that no input parameter values can be negative. Based on the adopted HF definition

(Eq. 1), the larger the value of HF, the more the input parameter values deviate from their original value, so contacts with values less than the weighted average in the base case will become progressively smaller as the heterogeneity factor is increased. Eventually, with a very large HF, these contacts' input values will deviate so far from their original value that they will become negative. Given this constraint, different HFs were chosen for contact peak tensile strength and block Poisson's ratio than the other input parameters. Additionally, a set of simulations were run where the values of all input parameters (block moduli and contact properties) were varied simultaneously according to the heterogeneity factor. The HFs used for each set of simulations are summarized in Table 6.

Note that the HF values that are less than 1 are equivalent to the reciprocals of the HF values greater than 1 for most input parameters, except for HF = 0. An exception is for block Poisson's ratio, where the reciprocals did not result in large enough changes in parameter values to make a significant difference in model inputs for each HF.

Residual friction angle and dilation angle are the remaining two input parameters tested that are not addressed in Table 6. This is because the heterogeneity factor described in Eq. 1 does not apply for these parameters, since all contact types were assigned the same value in the base case (see Table 3). Assigning the same value for residual friction angle and for dilation angle for all contacts in a polymineralic BBM is common (Farahmand and Diederichs 2015; Lan et al. 2010; Nicksiar and Martin 2014; Sinha and Walton 2020); in such a case, because the weighted average of all contacts is equal to the value assigned to all contacts, the difference between the contact's value and the weighted average is always zero. This term is multiplied by HF in Eq. 1, so no matter the value of HF input in Eq. 1, the resulting value will always be equal to the weighted average. Therefore, Eq. 1 does not apply to contact residual friction angle and dilation angle. Note that although BBMs require residual cohesion and residual tensile strength inputs as well, these were assumed to be zero for all contacts, as is common in models of brittle rock (Ghazvinian et al. 2014; Stavrou and Murphy 2018; Wang and Cai 2019).

Therefore, a different approach was used that set minimum and maximum range values for both of these contact parameters. These minimum and maximum values became progressively spaced further apart from each other, corresponding to an increase in heterogeneity (see Tables 7 and 8). The ten contact types within the BBM were ranked on the basis of their peak cohesion (see Table 3), where the contact type with a rank of 1 was assigned the maximum value and the contact type with a rank of 10 was assigned the minimum value. Peak cohesion is the input parameter that predominantly affects the overall strength of a contact (under low confinement conditions), so it was used to rank contacts on the basis of their strength. The eight contact types in between were assigned intermediate values between the maximum and minimum, following the order of rank, and maintaining the weighted average. The contact type rankings are also listed in Tables 7 and 8.

Each parameter set, corresponding to the HFs listed in Table 6 and to those listed in Tables 7 and 8, was assigned to the BBM in successive model runs, while all other input parameters were held constant (per Tables 2 and 3).

Table 6 Summary of the heterogeneity factors (HFs) used in the heterogeneity parametric study

Input parameter	Block properties		Contact properties					
	E	ν	jkn	jks	c	ϕ	jt	Overall
Heterogeneity factors (HF)	1	1	1	1	1	1	1	1
	1.25	1.15	1.25	1.25	1.25	1.25	1.10	1.15
	1.50	1.25	1.50	1.50	1.50	1.50	1.25	1.25
	1.75	1.35	1.75	1.75	1.75	1.75	1.40	1.35
	2.00	1.45	2.00	2.00	2.00	2.00	1.55	1.40
	0.80	0.80	0.80	0.80	0.80	0.80	0.91	1.45
	0.67	0.60	0.67	0.67	0.67	0.67	0.80	0.80
	0.57	0.40	0.57	0.57	0.57	0.57	0.71	0.60
	0.50	0.20	0.50	0.50	0.50	0.50	0.65	0.40
	0.40	0.15	0	0	0	0	0	0.20
	0.30	0.10						0.15
	0.10	0.05						0.10
	0	0						0

Definitions of parameter abbreviations are: E = Young's modulus, ν = Poisson's ratio, jkn = normal stiffness, jks = shear stiffness, c = cohesion, φ = friction angle, jt = tensile strength. Note that the HFs for block Poisson's ratio and contact tensile strength are different from those of the other input parameters due to the constraint discussed previously

Table 7 List of input values for residual friction angle in degrees

Ranking	Range	0	1	2	3	4	5
	Minimum	3.00	2.50	2.00	1.50	1.00	0.50
	Maximum	3.00	3.50	4.00	4.50	5.00	5.50
1	Quartz–Quartz	3.00	2.90	2.80	2.50	3.00	2.50
2	Plagioclase–Plagioclase	3.00	3.50	4.00	4.50	5.00	5.50
3	Feldspar–Feldspar	3.00	3.45	3.90	4.40	4.75	5.75
4	Feldspar–Plagioclase	3.00	2.80	2.60	2.10	2.00	2.00
5	Quartz–Plagioclase	3.00	3.35	3.70	4.30	4.25	4.50
6	Mica–Mica	3.00	2.70	2.40	1.70	1.25	1.50
7	Mica–Quartz	3.00	3.00	3.00	2.90	3.25	3.00
8	Feldspar–Quartz	3.00	3.25	3.50	4.20	4.00	4.00
9	Mica–Feldspar	3.00	3.10	3.20	3.50	3.75	3.50
10	Mica–Plagioclase	3.00	2.50	2.00	1.50	1.00	0.50

Each column corresponds to a different set of parameters, where the "Range" (minimum value subtracted from maximum value) indicates the level of heterogeneity. 0 range is the base case listed in Table 2

Table 8 List of input values for dilation angle in degrees

Ranking	Range	0	1	2	3	4	5	6	7	8	9
	Minimum	5.00	4.50	4.00	3.50	3.00	2.50	2.00	1.50	1.00	0.50
	Maximum	5.00	5.50	6.00	6.50	7.00	7.50	8.00	8.50	9.00	9.50
1	Quartz–Quartz	5.00	4.90	4.75	5.00	4.25	4.50	4.50	4.00	4.00	3.50
2	Plagioclase–Plagioclase	5.00	5.50	6.00	6.5	7.00	7.50	8.00	8.50	9.00	9.50
3	Feldspar–Feldspar	5.00	5.45	5.75	6.00	6.25	7.00	7.50	8.25	8.50	9.00
4	Feldspar–Plagioclase	5.00	4.80	4.50	4.50	4.25	4.00	3.50	3.00	3.00	2.25
5	Quartz–Plagioclase	5.00	5.35	5.75	6.00	6.25	6.75	7.00	7.25	8.00	8.50
6	Mica–Mica	5.00	4.70	4.50	4.25	3.50	3.50	2.50	2.75	2.00	1.50
7	Mica–Quartz	5.00	5.00	5.00	5.00	5.25	5.00	5.50	5.00	5.00	5.50
8	Feldspar–Quartz	5.00	5.25	5.50	5.75	6.00	6.25	6.25	6.75	7.25	7.50
9	Mica–Feldspar	5.00	5.10	5.25	5.25	6.00	5.75	6.25	6.50	6.50	6.25
10	Mica–Plagioclase	5.00	4.50	4.00	3.50	3.00	2.50	2.00	1.50	1.00	0.50

Each column corresponds to a different set of parameters, where the "Range" (minimum value subtracted from maximum value) indicates the level of heterogeneity. 0 range is the base case listed in Table 2

Two-dimensional UCS and triaxial test simulations with 12 MPa of confining pressure were run for each of the parameter set variations. These two confinement levels are the bounds of the confinement range for which the BBM was calibrated (West et al. 2020).

Boundary conditions restricting movement in the vertical direction were applied to the bottom of the model, which represents the base platen used in real laboratory tests. A constant velocity boundary condition of 0.01 m/s was applied to the top of the model to ensure quasi-static loading (note that this value is consistent with previous numerical studies and cannot be directly compared to loading velocities used in physical laboratory tests; Huang et al. (2019), Kazerani and Zhao (2010), Stavrou and Murphy (2018)). A uniform load was applied to the lateral boundaries to simulate confining pressure. In the UCS simulations, zero pressure was applied (i.e., no boundary condition), whereas the confined simulation applied 12 MPa of load.

3 Model Analysis

During simulations, average axial stress, average axial strain, average lateral strain, and the number of cracks failing in tension and shear were tracked to monitor macroscopic properties of the stress–strain behavior of the BBM. Stress was determined by calculating the average internal stress value within each zone of the BBM (blocks are discretized into continuous elements for computation, which are referred to as "zones"). Strains were calculated by computing the average displacement of the edge points of the BBM (in both the axial and lateral directions) from their original positions and then dividing by the original corresponding dimension of the specimen. The macroscopic properties monitored for this study were Young's modulus, Poisson's ratio, CI and CD parameters, UCS and peak strength, and peak dilation angle. The methods for

determining each of these properties from the model outputs are discussed in the following sections.

3.1 Young's Modulus and Poisson's Ratio

Macroscopic Young's modulus and Poisson's ratio are elastic parameters and are determined using the linear elastic portions of the axial strain and lateral strain data, respectively. Young's modulus was determined as the slope of the axial stress–axial strain curve within this linear elastic region (i.e., tangent Young's modulus (Małkowski and Ostrowski 2017)), and Poisson's ratio was determined as the slope of the lateral strain–axial strain curve within the linear elastic region.

3.2 Crack Initiation (CI) and Crack Damage (CD)

The crack initiation threshold is defined as the stress at the onset of systematic cracking, which is equivalent to the point of nonlinearity in the axial stress–lateral strain curve, as well as the point of reversal in crack volumetric strain. The crack damage stress threshold corresponds to the point at which isolated cracks begin to grow and interact, which is equivalent to the point of nonlinearity in the axial stress–axial strain curve (Diederichs and Martin 2010; Ghazvinian et al. 2012; Martin and Chandler 1994). In BBMs, the formation of cracks can be easily tracked during the simulation of the compression test; the formation of cracks is observed as failure of contacts between blocks in the BBM. In this case, CI can be determined from a tensile crack curve and CD can be determined from a shear crack curve by selecting the point of accelerated increase in the number of the respective cracks (Ghazvinian et al. 2014; Nicksiar and Martin 2014). Specifically, CI and CD are evaluated at the intersection of the second and third linear regions in the crack curve, where these linear segments are determined visually (Sinha and Walton 2020). Examples of CI and CD determination with this method as applied in this study are shown in Figs. 4 and 5, respectively.

3.3 UCS and Peak Strength

To distinguish between the results obtained in the unconfined and confined cases, the overall strength of the BBM when there is zero confining pressure is referred to as the "UCS," and the overall strength when there is 12 MPa confining pressure is referred to as the "peak strength". Strength is assessed by identifying the largest stress achieved by the BBM during the simulation.

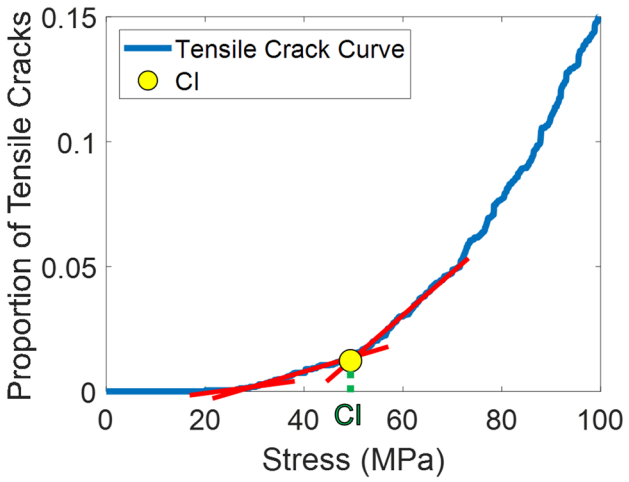

Fig. 4 Determination of the crack initiation (CI) parameter for the BBM using the tensile crack method. CI is approximately 47 MPa. "Proportion of Tensile Cracks" on the vertical axis is defined as the number of tensile cracks divided by the total number of tensile cracks formed during the simulation

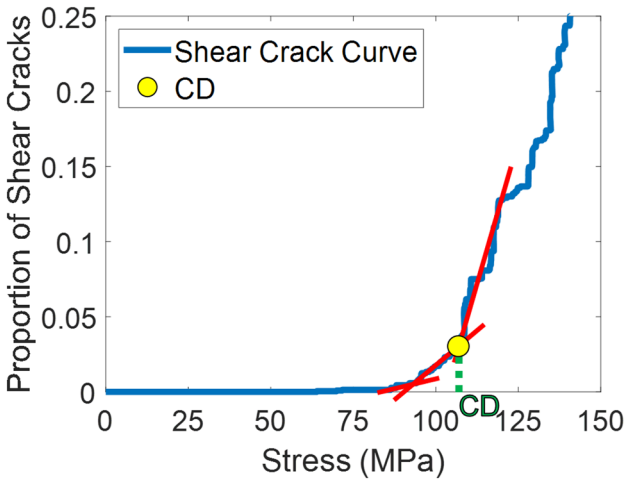

Fig. 5 Determination of the crack damage (CD) parameter for the BBM using the shear crack curve method. CD is approximately 109 MPa. "Proportion of Shear Cracks" on the vertical axis is defined as the number of shear cracks divided by the total number of shear cracks formed during the simulation

3.4 Peak Dilation Angle

Dilation angle is a mechanical property used to quantify the degree of volume increase as a rock specimen is loaded. The formation of cracks and void space between grains in the rock and the mobilization of friction via block movement and rotation results in a volume increase (Zhao and Cai 2010). Dilation angle is defined via Eq. 2:

$$\sin(\psi) = \frac{\dot{\varepsilon}_{v}^{p}}{-2\dot{\varepsilon}_{ax}^{p} + \dot{\varepsilon}_{v}^{p}} \tag{2}$$

where ψ is dilation angle, $\dot{\varepsilon}_v^p$ is incremental volumetric plastic strain, and $\dot{\varepsilon}_{ax}^p$ is incremental axial plastic strain (i.e., first principal plastic strain). Plastic strains are calculated by subtracting the linear elastic strain component from the total strain component (Walton et al. 2018). Volumetric strain is defined via Eq. 3:

$$\varepsilon_v = \varepsilon_{ax} + 2\varepsilon_{rad} \tag{3}$$

Equation 3 applies to volumetric strain in terms of total strain and plastic strain (like the variables in Eq. 2).

Dilation angle increases in the pre-peak, reaches its maximum value near the point of peak strength, and then decreases as more plastic shear strain is incurred. Only the peak dilation angle is considered for the purposes of this study.

4 Data Interpretation Method

For each model set, the macroscopic behaviors of the BBM under unconfined conditions and confined conditions with 12 MPa of confinement were analyzed, as discussed in Sect. 3. Outputs for each macroscopic property were normalized to the average value for each input parameter set, and the results were evaluated as a function of the heterogeneity factor (HF) (Eq. 1; Table 6) or range (Tables 7 and 8). An example of the normalization process is shown in Fig. 6.

It should be noted that although the data analysis has been performed using linear regression, a slight non-linear trend was noted in the majority of the results. Decreasing the heterogeneity from the base case (HF = 1) to HF values less than 1 appears to have a smaller effect on the macroscopic BBM property than increasing the heterogeneity from the base case to HF values greater than 1. This "kink" in the linear trend was typically observed to occur at or below HF = 1, which is the base (i.e., calibrated) input parameter set. Two examples of this bi-linear trend are shown in Fig. 7.

It is important to keep in mind that the linear model is not intended to be a predictive model due to the presence of this "kink." Rather, the linear model is simply meant to provide a first-order approximation of the degree to which a trend exists. For example, the slope of the model shown in Fig. 7a is much larger than the slope of the model shown in Fig. 7b. Therefore, it is clear that the heterogeneity of contact peak cohesion affects the unconfined CD of the BBM more than that of contact peak friction angle. Therefore, only linear regression models have been fit to the BBM results in this study.

5 Results and Discussion

It is important to note that the results of this parametric study only apply to one grain (i.e., block) structure. This grain structure dictates the arrangement of different block and contact types within the model. If multiple grain structure realizations for Blanco Mera granite were tested, the results would be expected to differ, although such differences would likely not be large enough to change the overall findings (Contreras Inga et al. 2021). The authors hypothesize that some of the apparently "random" variability in some of the following results is in fact related to the ways in which

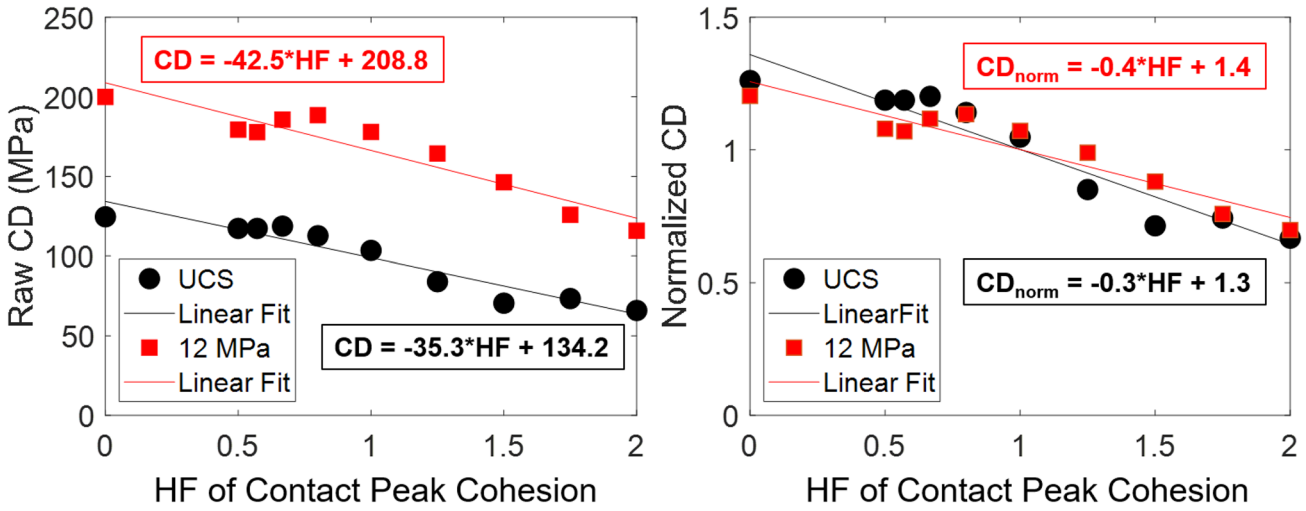

Fig. 6 Example of normalization of data and corresponding linear regression models. The raw data (left) for the CD of the BBM, as a function of the heterogeneity factor (HF) of contact peak cohesion, were normalized by dividing each raw data point by the average CD value for all HFs tested in the set. The average CD for the UCS tests was 98.8 MPa and the average CD for the confined tests with 12 MPa of confinement was 166.1 MPa. The normalized data are plotted on the right. Linear regression for both raw data and normalized data are included with their equations, for both confinement cases

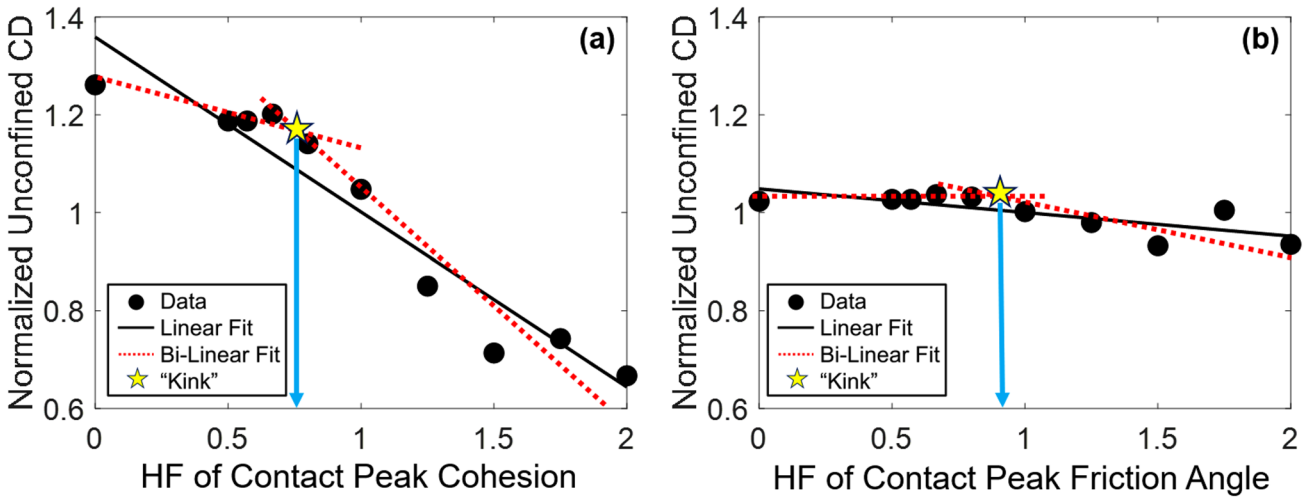

Fig. 7 Two examples of the non-linear trend observed in the majority of cases presented in Table 8. The results presented correspond to cases with varying heterogeneity in **a** contact peak cohesion and **b** contact peak friction angle. The black circles are unconfined CD values. The black solid line shows the linear fit and the red dashed lines show the bi-linear trend observed in the data. The intersection of the two linear portions is marked with a yellow star, and the corresponding HF is indicated by the blue arrow. Note that HF at which the kink was observed was found to consistently occur at or below HF = 1 (Color figure online)

changes in the heterogeneity of different properties influence the specific damage localization and failure pathways within the models, which is inherently related to the specific grain structure realization used.

Some non-linear trends were observed in the data, particularly for block Young's modulus and Poisson's ratio. More discussion on the effects that block elastic parameters have on the behavior of the BBM are included in Sect. 5.2.

5.1 Linear Trends as a Function of Heterogeneity in Individual Input Parameters

Visual assessment confirmed that the linear model discussed in Sect. 4 could approximately represent the trends of the results for most of the cases. Thus, a linear regression line was fit to the normalized data for each case, and a linear trend was considered notable if it had an R^2 value of at least 0.8 and a normalized percent trend absolute value of at least 5%. The trends that satisfy this requirement are summarized in Table 9. Note that a trend slope magnitude of 5% indicates that when the heterogeneity of the given input parameter is doubled, the model prediction for the output property being considered changes by 5%. Therefore, trend slope magnitudes lower than 5% signify a negligible change in the BBM's macroscopic property value as a function of heterogeneity of the given input parameter.

In examining the results shown in Table 9, it can be seen that the macroscopic material properties Young's modulus, Poisson's ratio, CI, confined peak strength, the ratio of CI to peak strength, and peak dilation angle were not notably affected by changing the heterogeneity of any individual contact input parameter. Additionally, the heterogeneity of contact stiffnesses, peak tensile strength, residual friction

Table 9 Summary of results (with R^2 of at least 0.8 and a normalized percent trend of at least 5%) of the macroscopic properties of the BBM that were affected by the heterogeneity of an individual input parameter

Macroscopic BBM property	Input parameter	Normalized trend	R^2
Young's modulus	–	–	–
Poisson's ratio	–	–	–
CI (UCS)	–	–	–
CI (12 MPa)	–	–	–
CD (UCS)	Peak cohesion	− 35.8%	0.92
CD (12 MPa)	Peak cohesion	− 25.6%	0.89
	Peak friction angle	− 7.6%	0.80
UCS	Peak cohesion	− 11.7%	0.85
Peak strength (12 MPa)	–	–	–
CI/UCS	–	–	–
CI/Peak strength (12 MPa)	–	–	–
CD/UCS	Peak cohesion	− 25.4%	0.84
CD/Peak strength (12 MPa)	Peak cohesion	− 30.3%	0.88
Peak dilation angle (UCS)	–	–	–
Peak dilation angle (12 MPa)	–	–	–

Normalized percent trend and R^2 values are calculated via linear regression (Fig. 5). A negative percent change indicates a decrease in the property's value when the model heterogeneity is increased

angle, and dilation angle had negligible effects on the BBM's behavior. In contrast, the heterogeneity of contact peak cohesion and peak friction angle was found to have a notable effect on the macroscopic behavior of the BBM, both of which will be discussed in the following sub-sections.

5.1.1 Peak Cohesion

The most notable finding of this parametric study is that the heterogeneity of contact peak cohesion has a large impact on CD values, both under unconfined and confined conditions. According to the linear regression models, one unit increase in HF resulted in a decrease of 35.8% in the BBM's CD under unconfined conditions, and a decrease of 25.6% in the case with 12 MPa of confinement (see Fig. 8).

The heterogeneity of contact peak cohesion was also found to affect the UCS of the BBM. According to the linear regression model, a unit increase in HF of peak cohesion decreased the BBM's UCS by 11.7% (see Fig. 9). Although the heterogeneity of contact peak cohesion has a non-negligible effect on the BBM's UCS, it has a much larger influence on the BBM's CD. It also did not have a notable effect on the confined peak strength of the BBM.

This same trend is observed when analyzing the ratio of CD to peak strength, where increasing HF by one unit decreased this ratio by 25.4% and 30.3% for the unconfined and confined cases, respectively, according to the linear regression models (see Fig. 10).

The average value of peak cohesion over all contact types in the BBM has previously been found to have a strong effect on both the UCS and CD of BBMs, where a higher average value of contact peak cohesion resulted in a higher UCS (Bahaaddini and Rahimi 2018; Cai and Noorani 2015) and higher CD (Wang and Cai 2019), under all confinement conditions. Since this parametric study has found that increasing the heterogeneity of contact peak cohesion decreases UCS and CD, it appears that the minimum value assigned to contact peak cohesion represents a major control on the macroscopic behavior of the BBM following the initiation of cracking.

As per Table 9, contact peak cohesion is the primary input parameter for which heterogeneity significantly affects the macroscopic results of the simulation. This result is consistent with the modeling approach applied by Itasca Consulting Group, which uses heterogeneous values for contact peak cohesion and tensile strength while setting the other input parameters to be homogeneous (Garza-Cruz et al. 2014; Garza-Cruz and Pierce 2014).

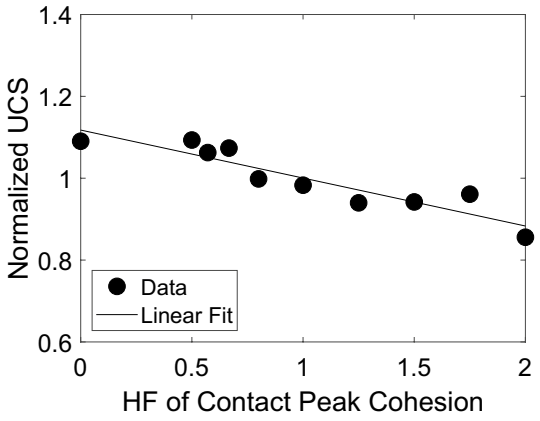

Fig. 9 Trend in the UCS of the BBM as a function of the variation of the heterogeneity of contact peak cohesion. Normalized trend = − 11.7%, $R^2 = 0.85$

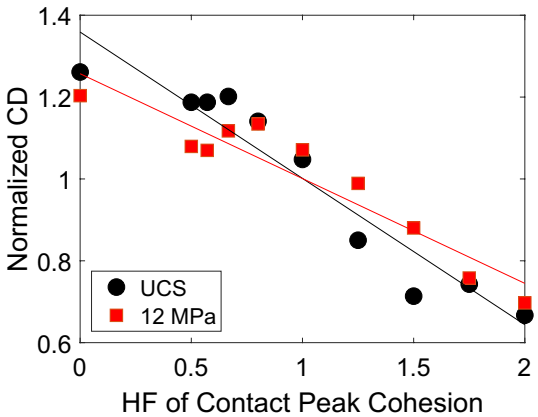

Fig. 8 Trend in unconfined (black circles) and confined (red squares) CD as a function of the heterogeneity variation of contact peak cohesion. Normalized trend = − 35.8%, $R^2 = 0.92$ for the unconfined case and normalized trend = − 25.6%, $R^2 = 0.89$ for the confined data (Color figure online)

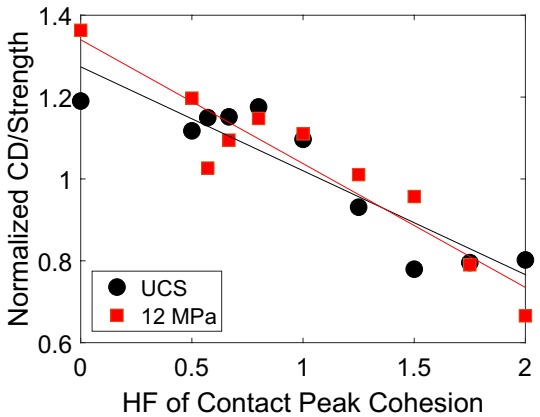

Fig. 10 Trend in unconfined (black circles) and confined (red squares) CD/peak strength ratio as a function of the heterogeneity variation of contact peak cohesion. Normalized trend = − 25.4%, $R^2 = 0.84$ for the unconfined data and normalized trend = − 30.3%, $R^2 = 0.88$ for the confined data (Color figure online)

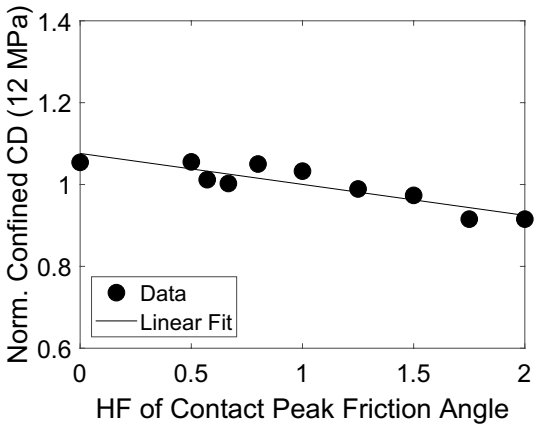

Fig. 11 Trend in confined CD as a function of the heterogeneity variation of contact peak friction angle. Normalized trend = − 7.6%, $R^2 = 0.80$

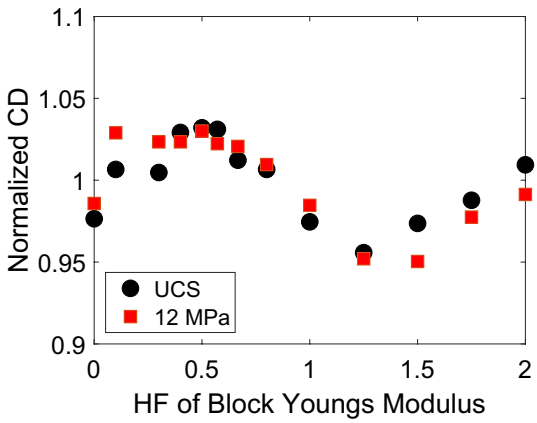

Fig. 12 Trend in CD for the unconfined (black circles) and confined with 12 MPa of confinement (red squares) cases as a function of the heterogeneity variation of block Young's modulus (Color figure online)

5.1.2 Peak Friction Angle

Compared to the effects of contact peak cohesion, the heterogeneity of contact peak friction angle was found to have a minor effect on the CD of the BBM. The linear regression model for CD under 12 MPa of confinement shows a decrease of 7.6% per unit increase in HF (see Fig. 11). The unconfined CD also exhibited a similar trend, but not a large enough trend to be included in Table 9.

The average value of peak friction angle over all contacts in the BBM has previously been found to have an effect on CD, where an increase in the average contact peak friction angle results in a higher CD, under all confinements (Farahmand and Diederichs 2015). Therefore, since increasing the heterogeneity of the input parameter values resulted in a decrease in CD, for both the UCS and triaxial test simulations, it appears that the minimum value assigned to contact friction angle is a notable control on the macroscopic behavior of the BBM.

5.2 Non-linear Influence of Elastic Block Parameters

As discussed previously, some trends were observed in the data that did not display a linear (or bi-linear) trend. These non-linear trends appeared as a result of varying the heterogeneity of the elastic block inputs parameters: Young's modulus and Poisson's ratio. These results are discussed in the following sub-sections.

5.2.1 Young's Modulus

The heterogeneity of block Young's modulus was found to have a non-linear effect on CD of the BBM (see Fig. 12).

It is important to note that the magnitude of the overall variations observed is not especially large. The range of normalized CD plotted on Fig. 12 is 0.9– 1.1, whereas the range of normalized values on all figures in Sect. 5.1 is 0.6–1.4. Given the lack of a clear physical explanation for this sinusoidal trend and its relatively small magnitude, it is plausible that the trend could be a numerical artifact related to the interaction between stiffness heterogeneity and some aspect of the solution process used in UDEC to run the simulations. Further investigation would be required to evaluate this hypothesis.

5.2.2 Poisson's Ratio

The heterogeneity of block Poisson's ratio was found to have a non-linear effect on the macroscopic Poisson's ratio of the BBM (see Fig. 13). Again, the magnitude of the normalized variation is relatively small.

The following explanation for the observed non-linear trend is postulated. For cases of small HFs (the left side

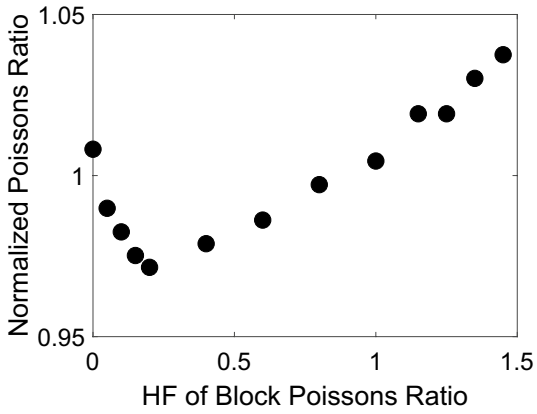

Fig. 13 Trend in macroscopic Poisson's ratio as a function of the heterogeneity variation of block Poisson's ratio

of Fig. 13), preferential elastic compaction of grains with low Poisson's ratios dominates the BBM's overall behavior. When a small amount of heterogeneity exists within the BBM, blocks with smaller Poisson's ratios are more capable of accommodating lateral deformation of the blocks with higher Poisson's ratios without generating significant axial stresses in response. This accommodation of lateral deformation means that less of the Poisson's effect of the higher Poisson's ratio grains leads to overall lateral expansion of the simulated specimen, resulting in a smaller macroscopic Poisson's ratio of the BBM. As HF increases, progressively larger local stresses are induced by the deformation of blocks with higher Poisson's ratios. Beyond a certain point (HF ≈ 0.2 in Fig. 13), preferential compaction of low Poisson's ratio grains is no longer the dominant micromechanical process during elastic deformation. Instead, a reversed trend is then observed for cases with high HFs (the right side of Fig. 13) where the blocks with high values of Poisson's ratio dominate the model's overall behavior, and the macroscopic Poisson's ratio is also high.

5.3 Influence of Varying Heterogeneity for All Parameters Simultaneously

The results of this parametric study discussed so far have indicated that the primary influence of input parameter heterogeneity on BBM macroscopic behavior is that of contact peak cohesion; specifically, CD decreases with increasing heterogeneity of this parameter. This finding is inconsistent with a previous study that found heterogeneity in BBMs is necessary to decrease confined CI and unconfined and confined CD to realistic levels relative to peak strength (Sinha and Walton 2020). For CD, homogeneous BBMs used in previous studies have exhibited unrealistically high values, where CD is often approximately coincident with the peak strength (Ghazvinian et al. 2014; Stavrou and Murphy 2018).

Sinha and Walton (2020) compared a completely homogeneous BBM to a completely heterogeneous BBM, but did not investigate varying degrees of heterogeneity within the BBM. With all this in mind, it was hypothesized that the impact of parameter heterogeneity on CI (and to a lesser extent CD) is not strongly associated with any individual input parameter, but rather with a combination of parameters. Accordingly, models were developed where multiple HF values were applied to all input parameters simultaneously, as described in Sect. 2. Specifically, each HF value was attributed to all elastic block properties and contact properties except for residual friction angle and dilation angle, as HF does not apply to these two parameters (these parameters were set to be fully homogeneous for these models). In this case, an HF equal to zero corresponds to a completely homogeneous BBM, where the input parameters are all equal to their weighted averages (see Sect. 2). An HF equal to 1 still represents the base case (see Tables 2 and 3).

Table 10 Summary of results (with R^2 of at least 0.8 and a normalized percent trend of at least 5%) of the macroscopic properties of the BBM that were affected by the heterogeneity of all input parameters, varied simultaneously

Macroscopic BBM property	Normalized trend	R^2
Young's modulus	–	–
Poisson's ratio	–	–
CI (UCS)	– 40.5%	0.90
CI (12 MPa)	– 27.2%	0.87
CD (UCS)	– 43.3%	0.96
CD (12 MPa)	– 27.3%	0.90
UCS	– 16.5%	0.97
Peak strength (12 MPa)	–	–
CI/UCS	– 24.3%	0.82
CI/Peak strength (12 MPa)	– 26.1%	0.85
CD/UCS	– 27.7%	0.88
CD/Peak strength (12 MPa)	– 26.2%	0.80
Peak dilation angle (UCS)	–	–
Peak dilation angle (12 MPa)	–	–

Normalized percent trend and R^2 values are calculated via linear regression (Fig. 5). A negative percent change indicates a decrease in the property's value as the heterogeneity increases

Visual assessment again confirmed that a linear model could approximate the trends of the results. Thus, a linear regression model was fit to the normalized data for each case, and a linear trend was presented if it had an R^2 value of at least 0.8 and a normalized percent trend absolute value of at least 5%. The trends that satisfy these requirements are summarized in Table 10.

The heterogeneity of the overall BBM was found to affect its macroscopic CI, the ratio of CI to peak strength, CD, the ratio of CD to peak strength, and UCS. Trends with respect to each macroscopic property are discussed in the following sub-sections.

5.3.1 Crack Initiation (CI)

The crack initiation (CI) threshold was affected by the overall heterogeneity of the BBM. According to the linear regression models, one unit increase in HF resulted in a decrease of 40.5% in the BBM's CI under unconfined conditions, and a decrease of 27.2% in the case with 12 MPa of confinement (see Fig. 14a and b). Additionally, the heterogeneity of the overall BBM affected the ratio of CI to peak strength similarly. According to the linear regression models, one unit increase in HF resulted in a decrease of 24.3% in the BBM's CI/UCS ratio, and a decrease of 26.1% in the case of CI/peak strength under 12 MPa of confinement (see Fig. 14c and d). The percent trend associated with unconfined CI (Fig. 14a)

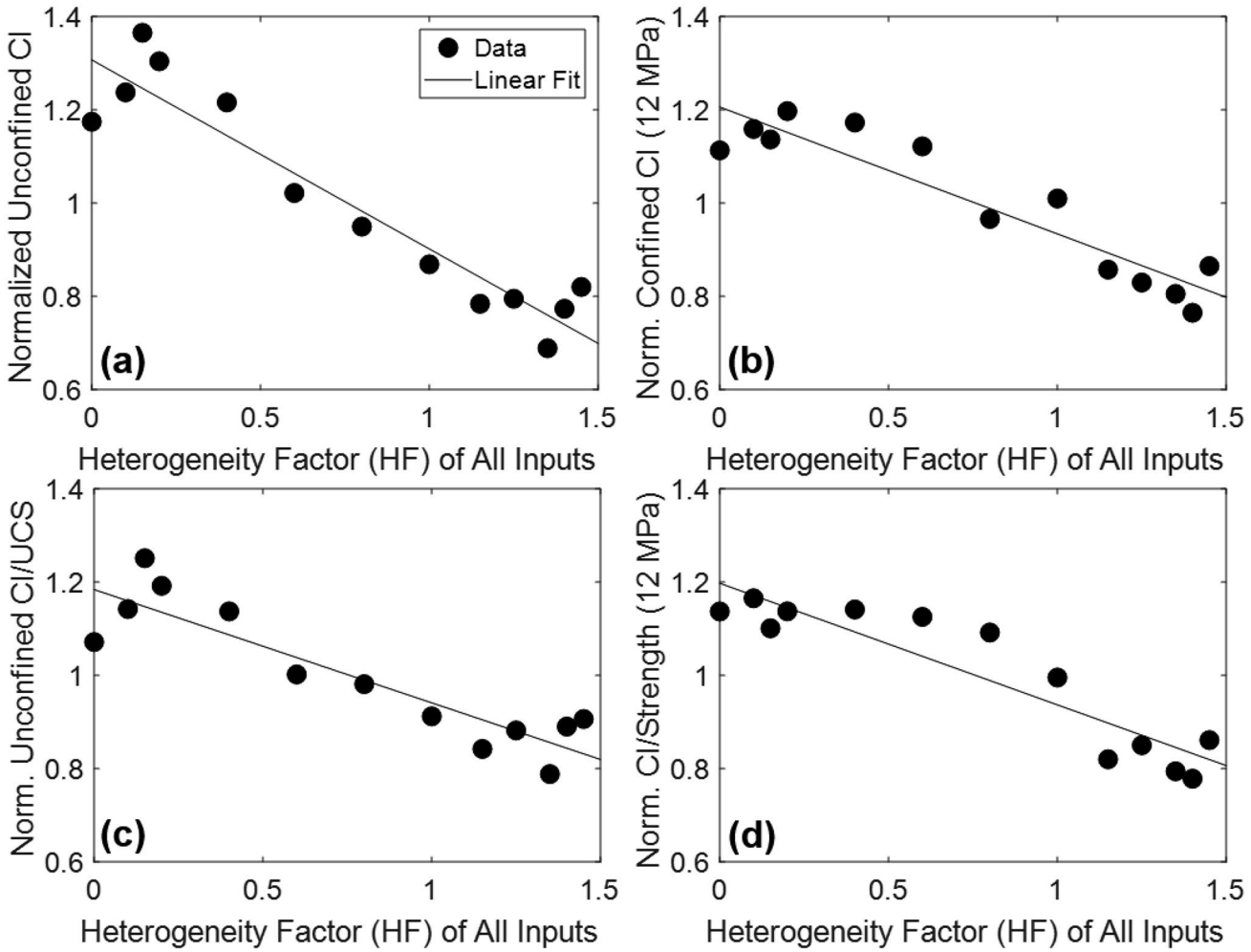

Fig. 14 CI (**a**, **b**) or the ratio of CI/peak strength (**c**, **d**) results plotted as a function of the heterogeneity factor (HF) applied to the entire BBM (all blocks and contact parameters). Unconfined results are included in (**a** and **c**) and confined results under 12 MPa of confinement are included in (**b** and **d**). **a** Normalized trend = − 40.5%, $R^2 = 0.90$, (**b**) normalized trend = − 27.2%, $R^2 = 0.87$, (**c**) normalized trend = − 24.3%, $R^2 = 0.82$, (**d**) normalized trend = − 26.1%, $R^2 = 0.85$

is notably higher than the percent trends of confined CI and the ratios of CI to peak strength (Fig. 14b through d).

These results confirm that the overall model heterogeneity does indeed exert a significant control on CI. To aid in the identification of which group of parameters was having the greatest influence on CI (in terms of heterogeneity), three extra sets of models were run under unconfined and confined conditions with 12 MPa of confinement: (1) models containing homogeneous blocks with heterogeneous contacts, (2) models containing heterogeneous blocks with homogeneous contact stiffness and heterogeneous contact strength, and (3) models containing heterogeneous blocks with heterogeneous contact stiffness and homogeneous contact strength. These cases are subsequently referred to as the "homogeneous blocks," "homogeneous contact stiffnesses", and "homogeneous contacts" models, respectively.

Compared to a fully homogeneous model (i.e., HF = 0), the homogeneous contacts model was found to have a similar unconfined CI value, whereas the homogeneous blocks model was found to have a similar confined CI value. This suggests that heterogeneity in contact strengths represents the primary influence of heterogeneity on CI under unconfined conditions, whereas heterogeneity of block stiffnesses represents the primary influence of heterogeneity on CI under confined conditions. In the unconfined case, local tensile stresses are widespread within the specimen due to the lack of lateral confinement (Diederichs 1999) and the influence of heterogeneity is dominated by that of the contacts. In the confined case, the spatial extent of local tension is reduced (Diederichs 1999), and therefore the most direct way to lower CI to realistic levels is by increasing stress-field heterogeneity through incorporation of heterogeneity in the elastic block properties. Note that this is consistent with the

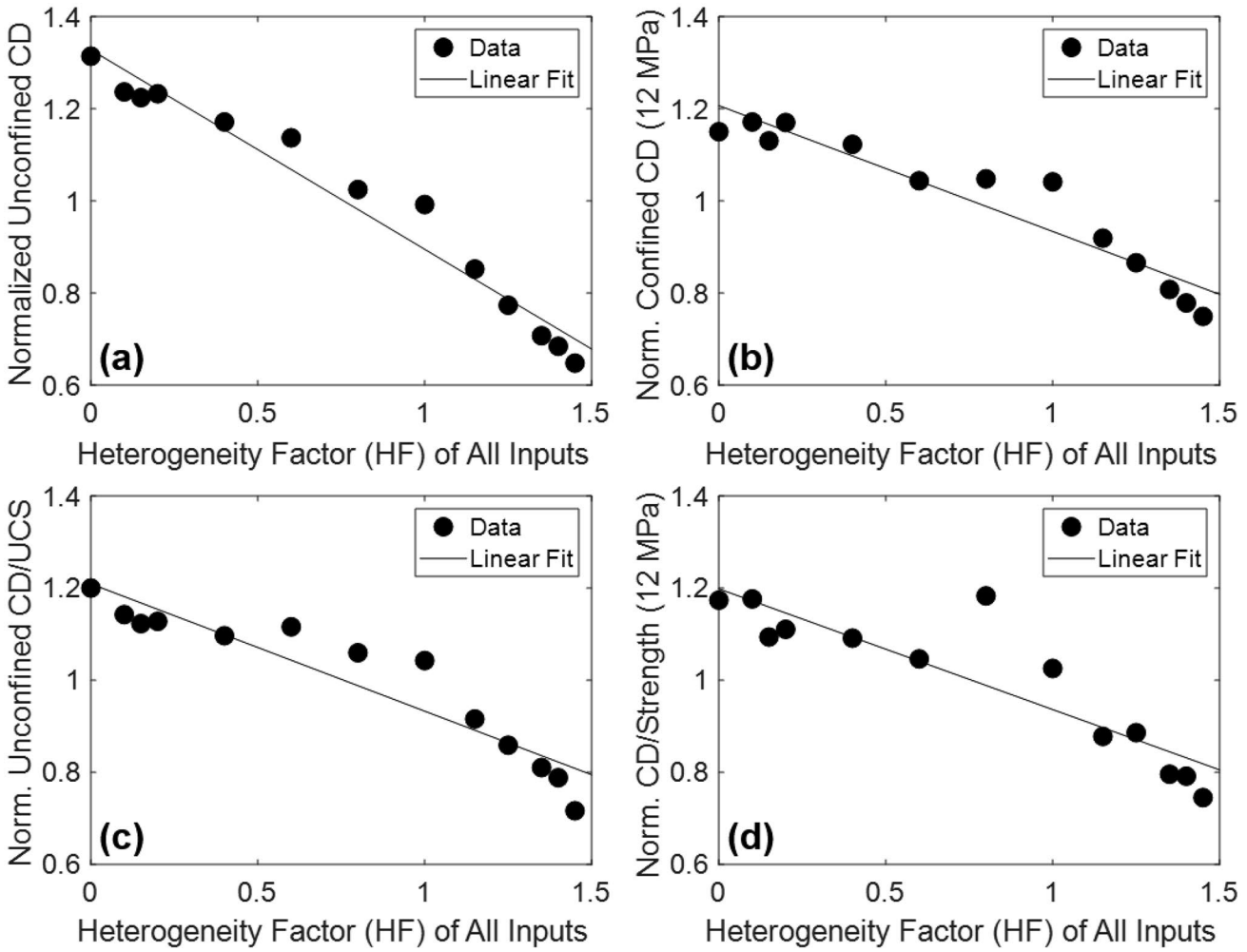

Fig. 15 CD (**a**, **b**) or the ratio of CD/peak strength (**c**, **d**) results plotted as a function of the heterogeneity factor (HF) applied to the entire BBM (all blocks and contact parameters). Unconfined results are included in (**a** and **c**) and confined results under 12 MPa of confinement are included in (**b** and **d**). **a** Normalized trend = − 43.3%, $R^2 = 0.96$, **b** normalized trend = − 27.3%, $R^2 = 0.90$, **c** normalized trend = − 27.7%, $R^2 = 0.88$, **d** normalized trend = − 26.2%, $R^2 = 0.80$

finding by Sinha and Walton (2020), who found that contact strength heterogeneity is not required to match CI (only stiffness heterogeneity is required) but contact strength heterogeneity does affect CI. In this study, it was found that contact tensile strength heterogeneity alone does not affect CI, but the heterogeneity of all model input parameters combined does have an effect.

5.3.2 Crack Damage (CD)

The crack damage (CD) threshold was also affected by the overall heterogeneity of the BBM. According to the linear regression models, one unit increase in HF resulted in a decrease of 43.3% in the BBM's CD under unconfined conditions, and a decrease of 27.3% in the case with 12 MPa of confinement (see Fig. 15a and b). Additionally, the heterogeneity of the overall BBM affected the ratio of CD to peak strength similarly. According to the linear regression models, one unit increase in HF resulted in a decrease of 27.7% in the BBM's ratio of CD to peak strength under unconfined conditions, and a decrease of 26.2% in the case with 12 MPa of confinement (see Fig. 15c and d).

These results are consistent with the behavior of BBMs in previous studies, where homogeneous BBMs had high values of CD relative to the peak strength (Ghazvinian et al. 2014; Stavrou and Murphy 2018; Sinha and Walton 2020) and heterogeneous BBMs were able to match laboratory CD values that are lower relative the peak strength (Farahmand and Diederichs 2015; Nicksiar and Martin 2014; Park et al. 2017; Sinha and Walton 2020).

These normalized percent trends are similar in value to those associated with contact peak cohesion heterogeneity (Table 9). Therefore, it appears that the heterogeneity of

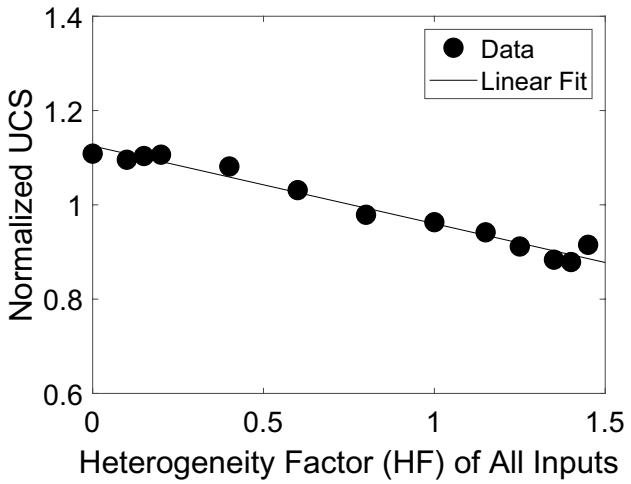

Fig. 16 UCS results plotted as a function of the heterogeneity factor applied to the entire BBM (all blocks and contact parameters). Normalized trend = − 16.5%, $R^2 = 0.97$

this input parameter has the most influence over the BBM. However, the trends are not identical, so the heterogeneity of other input parameters are affecting CD as well, but to a lesser extent.

5.3.3 Unconfined Compressive Strength (UCS)

The Unconfined Compressive Strength (UCS) of the BBM was affected by its overall heterogeneity. According to the linear regression model, one unit increase in HF resulted in a decrease of 16.5% in the BBM's UCS (see Fig. 16).

This normalized trend of –16.5% has a higher absolute value than the − 11.7% trend associated with contact peak cohesion heterogeneity (Table 9). Therefore, although the heterogeneity of other input parameters is affecting the BBM's UCS in addition to contact peak cohesion, contact peak cohesion heterogeneity remains the primary influence. It is also notable that the influence of overall model heterogeneity on peak strength did not extend to confined conditions.

6 Conclusion

A parametric study was conducted on the heterogeneity of elastic block and contact input parameters in bonded block models (BBMs). An elastic block BBM of Blanco Mera granite that had been previously calibrated to laboratory data (West et al. 2020) was used as the basis for this study, which includes four different mineral (block) types and ten distinct contact types. The input parameters for the elastic blocks are Young's modulus and Poisson's ratio. The input parameters for the contacts are normal and shear stiffnesses, peak cohesion, peak friction angle, peak tensile strength, residual friction angle, and dilation angle.

Each of these two elastic block properties and seven contact properties were tested separately by varying the degree of heterogeneity within a parameter type, while keeping the weighted average of the parameter constant for all simulations. Additional sets of input parameters were tested where the heterogeneity of all input parameters was varied simultaneously, while keeping their weighted averages constant.

Both a UCS test and a triaxial test with 12 MPa of confinement were simulated for each variation of the input parameters. Macroscopic material properties were computed from the model results including Young's modulus, Poisson's ratio, crack initiation (CI) and crack damage (CD) parameters, UCS and peak strength, and peak dilation angle. The following main findings were derived from model results:

- CI, confined peak strength, the ratio of CI/peak strength, and peak dilation angle were found to be insensitive to the heterogeneity of any individual input parameters.
- Although the macroscopic behavior of the BBM was found to be sensitive to the heterogeneity of multiple input parameters, only the heterogeneity of peak cohesion caused a large change in the model behavior (i.e., normalized percent trends of at least 25% in the linear regression models). Specifically, an increase in contact peak cohesion heterogeneity resulted in a decrease in CD of the BBM.
- The following smaller effects were also noted: contact peak cohesion heterogeneity influences UCS and contact peak friction angle heterogeneity influences CD under confined conditions.
- Elastic block moduli (Young's modulus and Poisson's ratio) were found to affect CD and macroscopic Poisson's ratio of the BBM, respectively, in a non-linear fashion, although the magnitudes of the trends observed were relatively small, and likely insignificant for practical purposes.
- Since previous studies in the literature noted that BBM heterogeneity was required to decrease both CI and CD of a BBM, it was hypothesized that the overall heterogeneity of the BBM would affect CI, rather than the heterogeneity of a single input parameter. Therefore, an additional parametric study was conducted where the heterogeneity of all input parameters was varied simultaneously (both blocks and contacts). Large changes were observed (i.e., normalized percent trends of at least 25% in the linear regression models) for UCS, CI, and CD as a function of overall BBM heterogeneity. Specifically, they were found to decrease with increasing heterogeneity.

Acknowledgements The authors would like to thank Itasca Consulting Group for providing educational licenses to UDEC, which were used to run some of the models for this study. The research conducted for this study was partially funded by the National Institute of Occupational Safety and Health (NIOSH) under Grant Number 200-2016-90154. The authors would like to extend their sincere gratitude for this financial support.

Author Contributions IW planned the study, setup and ran the simulations, analyzed data, and wrote the paper. GW assisted in planning and data analysis and edited the paper.

Funding The research conducted for this study was partially funded by the National Institute of Occupational Safety and Health (NIOSH) under Grant Number 200-2016-90154.

Data availability The data used in this study is available from the corresponding author, Isabella West, upon reasonable request.

Declarations

Conflict of Interest There are no conflicts of interest.

References

Alejano LR, Arzúa J, Bozorgzadeh N, Harrison JP (2017) Triaxial strength and deformability of intact and increasingly jointed granite samples. Int J Rock Mech Min Sci 95(May 2016):87–103. https://doi.org/10.1016/j.ijrmms.2017.03.009

Bahaaddini M, Rahimi M (2018) Distinct element modelling of the mechanical behavior of intact rocks using Voronoi tessellation model. Int J Min Geo-Eng 52(1):61–68

Bass JD (1995) Elasticity of minerals, glasses, and melts. In: Mineral physics & crystallography: a handbook of physical constant, 2nd edn

Cai M, Noorani R (2015) Simulation of dilation behavior of brittle rocks using a grain-based model. In: 13th International Congress of Rock Mechanics, Montreal, Canada, 6(May), 1–12. Retrieved from https://www.onepetro.org/conference-paper/ISRM-13CONGRESS-2015-050

Chen W, Konietzky H (2014) Simulation of heterogeneity, creep, damage and lifetime for loaded brittle rocks. Tectonophysics 633(1):164–175. https://doi.org/10.1016/j.tecto.2014.06.033

Chen W, Konietzky H, Tan X, Frühwirt T (2016) Pre-failure damage analysis for brittle rocks under triaxial compression. Comput Geotech 74(November 2017):45–55. https://doi.org/10.1016/j.compgeo.2015.11.018

Contreras Inga CE, Walton G, Holley E (2021) Statistical assessment of the effects of grain-structure representation and micro-properties on the behavior of bonded block models for brittle rock damage prediction. Sustainability (switzerland) 13(14):7889. https://doi.org/10.3390/su13147889

Diederichs MS (1999) Instability of hard rockmasses. University of Waterloo

Diederichs MS, Martin CD (2010) Measurement of spalling parameters from laboratory testing. In: Rock mechanics in civil and environmental engineering—proceedings of the european rock mechanics symposium, EUROCK 2010, pp 323–326. https://doi.org/10.1201/b10550-75

Fabjan T, Ivars DM, Vukadin V (2015) Numerical simulation of intact rock behaviour via the continuum and Voronoi tessellation models: A sensitivity analysis. Acta Geotechnica Slovenica 12(2):5–23

Farahmand K, Diederichs MS (2015) A calibrated synthetic rock mass (SRM) model for simulating crack growth in granitic rock considering grain scale heterogeneity of polycrystalline rock. In: 49th US rock mechanics/geomechanics symposium 2015, vol 1(i), pp 9–22

Garza-Cruz T, Pierce ME (2014) A 3DEC model for heavily veined massive rock masses. In: 48th US rock mechanics/geomechanics symposium 2014, vol 3, pp 2074–2082

Garza-Cruz T, Pierce ME, Kaiser PK (2014) Use of 3DEC to study spalling and deformation associated with tunnelling at depth. In: Proceedings of the seventh international conference on deep and high stress mining, pp 421–434. https://doi.org/10.36487/acg_rep/1410_28_garza-cruz

Garza-Cruz T, Pierce ME, Board M (2019) Effect of shear stresses on pillar stability: a back analysis of the troy mine experience to predict pillar performance at montanore mine. Rock Mech Rock Eng 52(12):4979–4996. https://doi.org/10.1007/s00603-019-02011-3

Ghazvinian E, Perras MA, Diederichs MS, Labrie D (2012) Formalized approaches to defining damage thresholds in brittle rock: granite and limestone. In: 46th US Rock Mechanics/Geomechanics Symposium 2012, vol 2, pp 966–974

Ghazvinian E, Diederichs MS, Quey R (2014) 3D random Voronoi grain-based models for simulation of brittle rock damage and fabric-guided micro-fracturing. J Rock Mech Geotech Eng 6(6):506–521. https://doi.org/10.1016/j.jrmge.2014.09.001

Huang F, Shen J, Cai M, Xu C (2019) An empirical UCS model for anisotropic blocky rock masses. Rock Mech Rock Eng 52(9):3119–3131. https://doi.org/10.1007/s00603-019-01771-2

Itasca Consulting Group Inc. (2014) UDEC universal distinct element code theory and background, 4th edn. Minneapolis, MN

Jing L (2003) A review of techniques, advances and outstanding issues in numerical modelling for rock mechanics and rock engineering. Int J Rock Mech Min Sci 40(3):283–353. https://doi.org/10.1016/S1365-1609(03)00013-3

Kazerani T, Zhao J (2010) Micromechanical parameters in bonded particle method for modelling of brittle material failure. Int J Numer Anal Methods Geomech 34:1877–1895. https://doi.org/10.1002/nag.884

Lan H, Martin CD, Hu B (2010) Effect of heterogeneity of brittle rock on micromechanical extensile behavior during compression loading. J Geophys Res. https://doi.org/10.1029/2009jb006496

Li J, Konietzky H, Frühwirt T (2017) Voronoi-based DEM simulation approach for sandstone considering grain structure and pore size. Rock Mech Rock Eng 50(10):2749–2761. https://doi.org/10.1007/s00603-017-1257-4

Li XF, Li HB, Zhao J (2019) The role of transgranular capability in grain-based modelling of crystalline rocks. Comput Geotech 110(January):161–183. https://doi.org/10.1016/j.compgeo.2019.02.018

Małkowski P, Ostrowski Ł (2017) The methodology for the young modulus derivation for rocks and its value. Procedia Eng 191:134–141. https://doi.org/10.1016/j.proeng.2017.05.164

Martin CD, Chandler NA (1994) The progressive fracture of Lac du Bonnet granite. Int J Rock Mech Min Sci Geomech Abstr 31(6):643–659. https://doi.org/10.1016/0148-9062(94)90005-1

Nicksiar M, Martin CD (2014) Factors affecting crack initiation in low porosity crystalline rocks. Rock Mech Rock Eng 47(4):1165–1181. https://doi.org/10.1007/s00603-013-0451-2

Park JW, Park C, Song JW, Park ES, Song JJ (2017) Polygonal grain-based distinct element modeling for mechanical behavior of brittle rock. Int J Numer Anal Meth Geomech 41(6):880–898. https://doi.org/10.1002/nag.2634

Quey R, Dawson PR, Barbe F (2011) Large-scale 3D random polycrystals for the finite element method: Generation, meshing and remeshing. Comput Methods Appl Mech Eng

200(17–20):1729–1745. https://doi.org/10.1016/j.cma.2011.01.002
Saito T (1981) Variation of physical properties of igneous rocks in weathering. ISRM Int Symp, IS 1981(September):191–196
Shen X, Arson C, Ferrier KL, West N, Dai S (2019) Mineral weathering and bedrock weakening: modeling microscale bedrock damage under biotite weathering. J Geophys Res Earth Surf 124(11):2623–2646. https://doi.org/10.1029/2019JF005068
Sinha S, Walton G (2020) A study on Bonded Block Model (BBM) complexity for simulation of laboratory-scale stress-strain behavior in granitic rocks. Comput Geotech 118(August 2019):103363. https://doi.org/10.1016/j.compgeo.2019.103363
Sinha S, Walton G (2021) Integration of three-dimensional continuum model and two-dimensional bonded block model for studying the damage process in a granite pillar at the Creighton Mine, Sudbury, Canada. J Rock Mech Geotech Eng 13(2):275–288. https://doi.org/10.1016/j.jrmge.2020.06.011
Stavrou A, Murphy W (2018) Quantifying the effects of scale and heterogeneity on the confined strength of micro-defected rocks. Int J Rock Mech Min Sci 102(November 2017):131–143. https://doi.org/10.1016/j.ijrmms.2018.01.019
Walton G, Alejano LR, Arzúa J, Markley T (2018) Crack damage parameters and dilatancy of artificially jointed granite samples under triaxial compression. Rock Mech Rock Eng 51(6):1637–1656. https://doi.org/10.1007/s00603-018-1433-1
Wang X, Cai M (2019) A comprehensive parametric study of grain-based models for rock failure process simulation. Int J Rock Mech Min Sci 115(February):60–76. https://doi.org/10.1016/j.ijrmms.2019.01.008
West IG, Walton G, Sinha S (2020) Simulating the behavior of compressively loaded blanco mera granite using bonded block models. In: Proccedings of the 54th US rock mechanics/geomechanics symposium
Zhao XG, Cai M (2010) A mobilized dilation angle model for rocks. Int J Rock Mech Min Sci 47(3):368–384. https://doi.org/10.1016/j.ijrmms.2009.12.007